

High-throughput analysis of Fröhlich-type polaron models

Pedro Miguel M. C. de Melo^{1,2}, Joao C. de Abreu², Bogdan Guster³, Matteo Giantomassi³, Zeila Zanolli¹, Xavier Gonze³, and Matthieu J. Verstraete²

¹*Chemistry Department, Debye Institute for Nanomaterials Science and European Theoretical Spectroscopy Facility, Condensed Matter and Interfaces, Utrecht University, PO Box 80.000, 3508 TA Utrecht, The Netherlands*

²*nanomat/Q-MAT/CESAM and European Theoretical Spectroscopy Facility, Université de Liège, B-4000 Liège, Belgium and*

³*UCLouvain, Institute of Condensed Matter and Nanosciences (IMCN), Chemin des Étoiles 8, B-1348 Louvain-la-Neuve, Belgium*

(Dated: July 4, 2022)

The electronic structure of condensed matter can be significantly affected by the electron-phonon interaction, which leads to important phenomena such as electrical resistance, superconductivity or the formation of polarons. This interaction is often neglected in band structure calculations, but can have a strong impact, e.g. on band gaps or optical spectra. Commonly used frameworks for electron-phonon energy corrections are the Allen-Heine-Cardona theory and the Fröhlich model. The latter accounts for a single longitudinal optical mode, a single parabolic electron band, and washes out atomic details. While it shows qualitative agreement with experiment for many polar materials, its simplicity should bring hard limits to its applicability in real materials. Improvements can be made by introducing a generalized version of the model, which takes into account anisotropic and degenerate electronic bands, and multiple phonon branches. In this work, we search for trends and outliers on over a thousand materials in existing databases of phonon and electron band structures. We use our results to identify the limits of applicability of the standard Fröhlich model by comparing to the generalized version, and by testing its basic hypothesis of a large radius for the polaronic wavefunction and the corresponding atomic displacement cloud (large polaron). The validity of the perturbative approach to the Fröhlich model is also tested. Among our extended set of materials, most exhibit large polaron behavior as well as validity of the perturbative treatment. However, especially for the valence band, there is also a significant fraction of the materials for which the perturbative treatment cannot be applied and/or for which the size of the self-trapping region is close to the atomic repetition distance. We find a large variety of behaviors, and employ much more accurate, fully ab initio Allen-Heine-Cardona calculations to understand extreme cases, where the Fröhlich model should fail and unusually large zero-point renormalization energies occur.

I. INTRODUCTION

The correct assessment of the electronic band gap and properties of charge carriers is of primary importance in determining the utility and applicability of semiconductors and insulators. Theoretical treatments usually only include the “frozen-ion” electronic aspect of the problem. Over the past two decades it has become clear that this is a severe limitation given the accuracy of both measurements and more advanced theory.^{1–9}

The most common band-gap calculations involve Kohn-Sham Density Functional Theory (KS-DFT)^{10–12} or the GW approximation from Many-body Perturbation Theory (MBPT), including different degrees of accuracy in the interactions between electrons^{13,14}. MBPT computations are more computationally demanding than KS-DFT, but can yield band-gap results that are within 2% to 10% of experimental measurements². However, both are zero-temperature formalisms: a crucial and often ignored effect is the electron-phonon interaction (EPI), which leads to a renormalization of the band-gap as a function of temperature. Even at $T = 0$ K, EPI yields the so called zero-point renormalization of the band gap (ZPR_{c+v}), that combines conduction and valence bands renormalizations (ZPR_c and ZPR_v).

Several theoretical approaches are available to calcu-

late the ZPR_{c+v} , among which the Fröhlich model¹⁵ and the perturbative formalism proposed in the Allen-Heine-Cardona (AHC) approach^{16–18}. In its first-principles version, AHC is the current gold standard for obtaining the ZPR_{c+v} ,^{3,4,6,7,19–23} although its computational load is quite large. In order for the AHC approach to be valid, the EPI should not be too strong, since it relies on a perturbative treatment.

In the original Fröhlich model, the charge carrier dynamics is described by a one-band isotropic and parabolic dispersion, and couples to one dispersionless longitudinal optical phonon mode. The EPI is accounted for in a rather coarse fashion with a fixed analytic functional form, thanks to the hypothesis that the electron-phonon interaction is dominated by the long-range behavior of the Coulomb interaction, in effect washing out all atomic details. Studies of this model have been numerous^{24–27}, and, depending on the EPI strength, can be done by perturbative means (weak coupling limit) or by a self-consistent approach to electron self-trapping by the phonon field (strong coupling limit). Some techniques allow to cover the entire coupling strength range,^{25,26} but are either difficult to generalize to first-principles approaches or require enormous computational resources.

The quasi-particle formed by a charge carrier dressed with phonons is called a “polaron”. Usually, the Fröh-

lich model is only considered for so-called “large” polarons, for which the atomic details are ignored, while the denomination “small polarons” corresponds to the case where the localization of the electronic wavefunction is comparable to interatomic distances. Interestingly, large polarons can be self-trapped as well, but in this case the self-trapping region is much larger than the interatomic distance.

More recently Miglio et al.⁹ derived a generalized Fröhlich model, capturing a more realistic physical picture than the standard Fröhlich model, in which one accounts for anisotropic and/or degenerate electronic dispersion, coupled to multiple phonons modes, possibly anisotropic, but still preserving the intrinsic continuum hypothesis (i.e. long-wavelength limit).

While for the Fröhlich model and its generalization only the zone-center phonons are needed, the AHC formalism requires the full phonon spectrum over the whole Brillouin Zone (BZ), and involves the explicit calculation of EPI matrix elements, making it computationally much more costly. ZPR_{c+v} determined via the generalized Fröhlich model have shown comparable results to the AHC formalism for a set of materials that include oxides and II-VI compounds. However for less ionic materials, its predictions are not on a par with AHC.⁹

The materials studied in this work will be primarily polar, thus the use of the (generalized) Fröhlich model is natural for two reasons: they are expected to yield polarons, and the model is a much less computationally costly estimation of the ZPR_{c+v} . Given the recent developments on the Fröhlich model⁹ and the prevalence of polarons in different classes of semiconducting materials²⁸, a thorough evaluation of the standard and generalized Fröhlich models over a broad range of materials is essential in order to establish each model’s validity and limiting behaviors. One intrinsic aspect to the Fröhlich model is the continuum limit, i.e. ignoring the crystal details while assuming that the polaron wavefunction is much larger than the shortest distance between atoms: the assumption is that one deals with large polarons. Other models are more suitable to include some level of atomistic detail, such as the Holstein model^{29,30}, which is not discussed here. Independently of the length-scale aspect of the polaron problem, a qualitative criterion arises within the original Fröhlich model with coupling strength α . In a weak-coupling perturbative treatment of this model, at $\alpha \approx 6$ a breakdown occurs with the divergence of the effective mass. This is to say that beyond this point simple perturbation theories fail, and the polaron experiences an intermediate or strong coupling with the crystal lattice deformations. Below this qualitative limit, in the weak coupling limit ($\alpha < 6$), the straight perturbative approach to the Fröhlich model is in reasonably good agreement with more refined approaches such as Feynman’s path integral variational approach²⁵ or diagrammatic Monte Carlo²⁶. If the Fröhlich model for a given material points to a breakdown of the perturbative approach, it is likely that its AHC treatment is also

bound to fail, since it is based on a similar perturbative hypothesis.

The overall goal of this work is to exploit existing datasets from the literature to evaluate the breadth of applicability of the Fröhlich model(s). The development of high throughput workflows and database Application Programming Interfaces allows for fast queries of available information, allowing one to perform quick higher level calculations and even train machine learning algorithms. In this work, we rely on the database from Ref. 31, which provides the electronic band structure, geometry, dielectric tensors, and phonon properties (e.g. mode frequencies, eigendisplacements) for a set of 1521 semiconducting materials. These were selected according to the following criteria: from two to five chemical elements per unit cell; experimentally stable 3D structures; non-magnetic; insulating materials with a minimal DFT band gap. The missing data on band masses is computed via a high throughput computational flow employing both AbiPy and ABINIT as described in Sec. IID. In the end, 1260 materials had all needed quantities to parameterize a Fröhlich model Hamiltonian. The remaining 261 materials either have unstable phonon modes or their band extrema were not located along high-symmetry lines in the BZ. The latter issue makes automating the computation of band effective masses extremely difficult, as one has to find the global maximum (minimum) of the valence (conduction) band in the BZ. We do not believe that their inclusion in this work would significantly alter the results shown herein.

We focus on indicators that could mark the potential of a material as a system with large or small polarons. These may be desirable (for optical properties) or undesirable (for transport) in different applications: more is not necessarily better. The essential quantity in the standard Fröhlich model α , and the parameters of its generalized form⁹, involve the dielectric tensor, the effective masses at the band extrema, the Born effective charge tensor, and the phonon frequencies, all of which are stored in the databases mentioned above.

The paper is structured as follows: in Sec. IIA we recap the theoretical background for the original Fröhlich model in describing large polarons, while in Sec. IIB we summarize the recent developments of the generalized Fröhlich model. We present the high-throughput results for the 1260 studied materials in Sec. III. We follow with Sec. IV by performing an *ab initio* validation using the AHC approach for selected materials, and we discuss outliers found using the Fröhlich model, such as materials with large ZPR and small coupling α , as well as materials with large ZPR and large α . In these cases the Fröhlich model should be treated in the strong-coupling limit, and the long-wavelength limit may fail entirely (these are two distinct cases). We conclude in Sec. V.

II. THEORY

A. The standard Fröhlich model

The Fröhlich model^{15,32} assumes a system with a single parabolic electron band of effective isotropic mass m^* and a single non-dispersive longitudinal optical phonon branch of frequency ω_{LO} . The electron-phonon interaction comes from the macroscopically screened Coulomb interaction between electrons and the nuclei moving along the optical phonon mode. While the latter approximation is dominant and qualitatively correct for $\mathbf{q} \approx 0$, it is assumed to be valid in the whole Brillouin zone, which corresponds to a continuum treatment, in line with the hypotheses of an isotropic electronic band and non-dispersive phonons. This means that there are no Debye-Waller contributions to the electron-phonon interaction, and transverse optical or acoustic modes are ignored. This model also ignores band degeneracies and the possibility of different band masses and warping.³³ Although formulated initially for a conduction electron, it can be easily applied to valence electrons, with a proper change of sign in selected formulas.

For a material with non-degenerate isotropic band extrema and isotropic dielectric function, we can write the following Hamiltonian for the standard Fröhlich model for an electron (conduction band - in atomic units $\hbar=1$, $a_{\text{Bohr}}=1$, $m=1$).³⁴

$$\hat{H}^{\text{sFr}} = \sum_{\mathbf{k}} \frac{\mathbf{k}^2}{2m^*} \hat{c}_{\mathbf{k}}^\dagger \hat{c}_{\mathbf{k}} + \sum_{\mathbf{q}} \omega_{\text{LO}} \hat{a}_{\mathbf{q}}^\dagger \hat{a}_{\mathbf{q}} + \sum_{\mathbf{k}, \mathbf{q}} g^{\text{sFr}}(\mathbf{q}) \hat{c}_{\mathbf{k}+\mathbf{q}}^\dagger \hat{c}_{\mathbf{k}} (\hat{a}_{\mathbf{q}}^\dagger + \hat{a}_{-\mathbf{q}}), \quad (1)$$

where the electron-phonon coupling constant is given by

$$g^{\text{sFr}}(\mathbf{q}) = \frac{1}{q} \left(\frac{2\pi\omega_{\text{LO}}}{\epsilon^* V_{\text{BvK}}} \right)^{\frac{1}{2}} = \frac{1}{q} \left(\frac{2\sqrt{2}\pi}{V_{\text{BvK}}} \frac{\omega_{\text{LO}}^{3/2}}{\sqrt{m^*}} \alpha \right)^{\frac{1}{2}}, \quad (2)$$

V_{BvK} is the Born von Kármán supercell volume, the dimensionless coupling parameter α is

$$\alpha = \frac{1}{\epsilon^*} \sqrt{\frac{m^*}{2\omega_{\text{LO}}}}, \quad (3)$$

where ϵ^* is defined by

$$\frac{1}{\epsilon^*} = \frac{1}{\epsilon^\infty} - \frac{1}{\epsilon^0}. \quad (4)$$

As a side note, ϵ^* , ϵ^∞ and ϵ^0 are independent of the nuclear masses: ϵ^∞ is purely electronic, while ϵ^0 is obtained in the adiabatic limit (low-frequency limit), so that the nuclei have time to adjust adiabatically to the applied electric field, regardless of their mass. ϵ^* is always greater than ϵ^∞ . For polar compounds with strong ionic screening, the difference in ϵ 's will be large, and $\epsilon^* \rightarrow \epsilon^\infty$

whereas for purely covalent compounds or mono-atomic compounds $\epsilon^0 \simeq \epsilon^\infty$, and so $\epsilon^* \rightarrow \infty$, which runs counter to intuition for habitual dielectric responses, but simply pushes α to 0 in the Fröhlich model. In Eqs. (1) and (4), we follow the Born and Huang convention for the phonon eigenvectors at \mathbf{q} and $-\mathbf{q}$.³⁵

The Hamiltonian in Eq. (1) can be simplified by using a different choice of units:

$$\hat{H}^{\text{sFr}} = \sum_{\mathbf{k}} \frac{\mathbf{k}^2}{2} \hat{c}_{\mathbf{k}}^\dagger \hat{c}_{\mathbf{k}} + \sum_{\mathbf{q}} \hat{a}_{\mathbf{q}}^\dagger \hat{a}_{\mathbf{q}} + \sum_{\mathbf{k}, \mathbf{q}} \frac{1}{q} \left(\frac{2\sqrt{2}\pi\alpha}{V_{\text{BvK}}} \right)^{\frac{1}{2}} \hat{c}_{\mathbf{k}+\mathbf{q}}^\dagger \hat{c}_{\mathbf{k}} (\hat{a}_{\mathbf{q}}^\dagger + \hat{a}_{-\mathbf{q}}), \quad (5)$$

where the energies, momenta, and length were rescaled by factors of ω_{LO} , $(\omega_{\text{LO}} m^*)^{1/2}$, and $(\omega_{\text{LO}} m^*)^{-1/2}$, respectively. With this choice, it becomes clear that the sole free parameter α characterizes the strength of the electron-phonon interaction with respect to the intrinsic electron and phonon terms.

Such a Hamiltonian can be treated by perturbation theory, in the limit of small α , delivering the polaron binding energy (ZPR) (again in atomic units instead of ω_{LO} units) as

$$E_{\text{P}} = -\omega_{\text{LO}}(\alpha + 0.0159\alpha^2 + \dots). \quad (6)$$

A more accurate approach based on the Feynman path integral²⁵ can be employed, covering the whole range of coupling strengths, as follows:

$$E_{\text{P}} = -\omega_{\text{LO}}(\alpha + 0.98(\alpha/10)^2 + 0.60(\alpha/10)^3 + 0.14(\alpha/10)^4), \alpha \leq 5 \quad (7)$$

$$E_{\text{P}} = -\omega_{\text{LO}}(0.106\alpha^2 + 2.83), \alpha \geq 5.$$

With the same perturbative treatment, it is possible to show that the ratio between the effective masses of the polaron, m_{P}^* , and the electron is approximately given by

$$\frac{m_{\text{P}}^*}{m^*} = \left(1 - \frac{\alpha}{6} + 0.00417\alpha^2 + \dots \right)^{-1}. \quad (8)$$

At the lowest order of perturbation theory, one obtains the well-known formula

$$E_{\text{P}} \approx -\alpha\omega_{\text{LO}}, \quad (9)$$

or more explicitly,

$$E_{\text{P}} = -\frac{1}{\epsilon^*} \sqrt{\frac{m^* \omega_{\text{LO}}}{2}}, \quad (10)$$

where ω_{LO} contains the only dependence on nuclear masses. At this order in the expansion Eq. (8) yields the following polaron mass:

$$\frac{m_{\text{P}}^*}{m^*} \approx \left(1 - \frac{\alpha}{6} \right)^{-1}. \quad (11)$$

with the immediate consequence that at $\alpha = 6$ the polaron mass diverges and this low-order perturbation theory approach is no longer valid. This parameter thus also provides a breakdown point for the lowest-order perturbative treatment of the Fröhlich model. A large α is physically associated with the appearance of self-localization of the electron due to the phonon response, a non-perturbative phenomenon that can be treated, alternatively, in the so-called “strong-coupling” limit of the Fröhlich model. Thus the $\alpha = 6$ value suggests a change of regime for the Fröhlich polaron. Nevertheless the occurrence of the wide range of behaviors present in our set of 1260 materials demands a more careful treatment in describing the polaron effective mass: we make use of the results based on the Diagrammatic Monte Carlo method applied to the standard Fröhlich model²⁶, by mapping the corresponding electronic and polaronic effective masses in the available range of α (see Fig. 5 in Ref. 26). Outside of the available range we fit a smooth and continuous quartic function with a resulting best fit as follows:

$$\frac{m_P^*}{m^*} = (1.07\alpha^4 - 160.53)^{-1}. \quad (12)$$

The self-localisation of the electron yields the notion of a “polaron radius”, a_P . For instance, with a Gaussian ansatz for the electronic wavefunction, in the adiabatic limit one obtains:

$$\phi(\mathbf{r}) = \left(\frac{1}{a_P \sqrt{\pi}} \right)^{\frac{3}{2}} \exp \left(-\frac{\mathbf{r}^2}{2a_P^2} \right), \quad (13)$$

with

$$a_P = 3 \sqrt{\frac{\pi}{2}} \frac{\epsilon^*}{m^*}. \quad (14)$$

Coherently, a_P is defined only in terms of quantities that do not depend on the nuclear masses. When a_P is on the order of the distance between equivalent atomic sites in the crystals, the Fröhlich model cannot be a good representation of the real material, as it is based on a continuum hypothesis for the vibrational degrees of freedom.

B. The generalized Fröhlich model

The Fröhlich model can be generalized to include systems with degenerate and anisotropic band extrema, multiple phonon branches, and anisotropic dielectric functions⁹. Bands are still assumed to be parabolic in each direction and phonon energies are still constant with respect to the wave vector length \mathbf{q} , but all might depend on the direction. As in Ref. 36, we treat both conduction and valence bands thanks to the integer variable σ , that is 1 for the conduction band (or electron polarons), and -1 for the valence band (or hole polarons). The Hamiltonian is then similar to that of Eq. (1),

$$\hat{H}^{\text{gFr}} = \sum_{\mathbf{k}n} \frac{\sigma \mathbf{k}^2}{2m_n^*(\hat{\mathbf{k}})} \hat{c}_{\mathbf{k}n}^\dagger \hat{c}_{\mathbf{k}n} + \sum_{\mathbf{q}j} \omega_{j0}(\hat{\mathbf{q}}) \hat{a}_{\mathbf{q}j}^\dagger \hat{a}_{\mathbf{q}j} + \sum_{\mathbf{q}j, \mathbf{k}n'n} g^{\text{gFr}}(\mathbf{q}j, \mathbf{k}n'n) \hat{c}_{\mathbf{k}+\mathbf{q}n'}^\dagger \hat{c}_{\mathbf{k}n} \left(\hat{a}_{\mathbf{q}j}^\dagger + \hat{a}_{-\mathbf{q}j} \right), \quad (15)$$

with $m_n^*(\hat{\mathbf{k}})$ the direction-dependent effective masses, \mathbf{k} the electron wavevector, n the band index, $\omega_{j0}(\hat{\mathbf{q}})$ the direction-dependent phonon frequency, \mathbf{q} the phonon wavevector and j the phonon branch index. The electron-phonon coupling constant is given by

$$g^{\text{gFr}}(\mathbf{q}j, \mathbf{k}n'n) = \frac{i}{q} \frac{4\pi}{\Omega_0} \left(\frac{1}{2\omega_{j0}(\hat{\mathbf{q}}) V_{\text{BvK}}} \right)^{1/2} \frac{\hat{\mathbf{q}} \cdot \mathbf{p}_j(\hat{\mathbf{q}})}{\epsilon^\infty(\hat{\mathbf{q}})} \times \sum_m s_{n'm}(\hat{\mathbf{k}}') (s_{nm}(\hat{\mathbf{k}}))^*. \quad (16)$$

In these equations, the sum over n , n' and m runs only over the bands that connect to the degenerate extremum, that are renumbered from 1 to n_{deg} . The electron-phonon part also depends only on few quantities: the Born effective charges (entering the mode-polarity vectors \mathbf{p}_j which are the Born charge weighted phonon displacement vectors), the macroscopic dielectric tensor ϵ^∞ , and the phonon frequencies ω_{j0} , the primitive cell volume Ω_0 , the Born-von Karman normalization volume V_{BvK} corresponding to the \mathbf{k} and \mathbf{q} samplings. The s_{nm} tensors are symmetry-dependent unitary matrices, similar to spherical harmonics. Finally, $\mathbf{k}' = \mathbf{k} + \mathbf{q}$.

In this generalized model, the ZPR for a band extremum can be obtained also at lowest order of perturbation theory, as

$$\text{ZPR}^{\text{gFr}} = - \sum_{jn} \frac{\sigma}{\sqrt{2}\Omega_0 n_{\text{deg}}} \int_{4\pi} d\hat{\mathbf{q}} (m_n^*(\hat{\mathbf{q}}))^{1/2} \times (\omega_{j0}(\hat{\mathbf{q}}))^{-3/2} \left(\frac{\hat{\mathbf{q}} \cdot \mathbf{p}_j(\hat{\mathbf{q}})}{\epsilon^\infty(\hat{\mathbf{q}})} \right)^2. \quad (17)$$

When comparing with the expression for the renormalization energy from the standard Fröhlich model, Eq. (9), we see that it is possible to re-write Eq. (17) in a similar way, highlighting the fact that this expression originates from an average over $\hat{\mathbf{q}}$ directions, and summation over the contributions from different phonon branches;

$$\text{ZPR}^{\text{gFr}} = -\sigma \sum_j \langle \alpha_j(\hat{\mathbf{q}}) \omega_{j0}(\hat{\mathbf{q}}) \rangle_{\hat{\mathbf{q}}}, \quad (18)$$

where

$$\langle f(\hat{\mathbf{q}}) \rangle_{\hat{\mathbf{q}}} = \frac{1}{4\pi} \int_{4\pi} d\hat{\mathbf{q}} f(\hat{\mathbf{q}}) \quad (19)$$

is an average over $\hat{\mathbf{q}}$ directions.

The $\alpha_j(\hat{\mathbf{q}})$ parameters are defined by

$$\alpha_j(\hat{\mathbf{q}}) = \frac{4\pi}{\sqrt{2}\Omega_0} \left(\frac{1}{n_{\text{deg}}} \sum_{n=1}^{n_{\text{deg}}} (m_n^*(\hat{\mathbf{q}}))^{1/2} \right) \times (\omega_{j0}(\hat{\mathbf{q}}))^{-1/2} \left(\frac{\hat{\mathbf{q}} \cdot \mathbf{p}_j(\hat{\mathbf{q}})}{\epsilon^\infty(\hat{\mathbf{q}})\omega_{j0}(\hat{\mathbf{q}})} \right)^2, \quad (20)$$

and can also be re-written to look similar to Eq. (3),

$$\alpha_j(\hat{\mathbf{q}}) = \frac{\langle (m_n^*(\hat{\mathbf{q}}))^{\frac{1}{2}} \rangle_n}{\epsilon_j^*(\hat{\mathbf{q}}) \sqrt{2\omega_{j0}(\hat{\mathbf{q}})}} \quad (21)$$

where

$$\frac{1}{\epsilon_j^*(\hat{\mathbf{q}})} = \frac{4\pi}{\Omega_0} \left(\frac{\hat{\mathbf{q}} \cdot \mathbf{p}_j(\hat{\mathbf{q}})}{\epsilon^\infty(\hat{\mathbf{q}})\omega_{j0}(\hat{\mathbf{q}})} \right)^2 \quad (22)$$

replaces Eq. (4), while

$$\langle (m_n^*(\hat{\mathbf{q}}))^{\frac{1}{2}} \rangle_n = \frac{1}{n_{\text{deg}}} \sum_{n=1}^{n_{\text{deg}}} (m_n^*(\hat{\mathbf{q}}))^{1/2} \quad (23)$$

highlights that the effective mass entering Eq. (21) is an average over bands that are degenerate at the extremum.

To summarize, in the lowest order of perturbation theory treatment, the multiband, multibranch, anisotropic generalization of the simple Eq. (3) can be structured in the same way, with the band contribution being averaged, the branch contributions being summed, and the anisotropy being treated by an average over $\hat{\mathbf{q}}$ directions. The polaron formation energy writes

$$E_P = - \sum_j \left\langle \frac{\langle (m_n^*(\hat{\mathbf{q}}))^{\frac{1}{2}} \rangle_n}{\epsilon_j^*(\hat{\mathbf{q}})} \sqrt{\frac{\omega_{j0}(\hat{\mathbf{q}})}{2}} \right\rangle_{\hat{\mathbf{q}}}. \quad (24)$$

Note that σ does not appear in E_P .

A generalization of α to anisotropic, multibranch systems, $\alpha_j(\hat{\mathbf{q}})$, has been tentatively defined by C. Verdi, see Ref. 37, Eq.(4.12) page 62, however lacking both effective mass and phonon frequency dependencies on direction, and ignoring the possible electronic degeneracy.

From Eq. (24) one might examine the relevance of the following approximate decoupling between electronic and vibrational and dielectric contributions :

$$E_P \approx - \langle (m_n^*(\hat{\mathbf{q}}))^{\frac{1}{2}} \rangle_{\hat{\mathbf{q}}n} \left(\sum_j \left\langle \frac{1}{\epsilon_j^*(\hat{\mathbf{q}})} \sqrt{\frac{\omega_{j0}(\hat{\mathbf{q}})}{2}} \right\rangle_{\hat{\mathbf{q}}} \right). \quad (25)$$

The factorization of the $\langle (m_n^*(\hat{\mathbf{q}}))^{\frac{1}{2}} \rangle_{\hat{\mathbf{q}}n}$ term appears naturally and is exact in the cubic case.

C. The generalized Fröhlich model in cubic systems

For a cubic system, even with several phonon branches, there is no dependence on the direction of \mathbf{q} for the

phonon frequencies and dielectric properties. The Hamiltonian becomes^{35,36}

$$\hat{H}^{\text{cFr}} = \sum_{\mathbf{k}n} \frac{\sigma \mathbf{k}^2}{2m_n^*(\mathbf{k})} \hat{c}_{\mathbf{k}n}^\dagger \hat{c}_{\mathbf{k}n} + \sum_{\mathbf{q}j} \omega_{j\text{LO}} \hat{a}_{\mathbf{q}j}^\dagger \hat{a}_{\mathbf{q}j} + \sum_{\mathbf{k}n', \mathbf{q}j} g^{\text{cFr}}(\mathbf{q}j, \mathbf{k}n') \hat{c}_{\mathbf{k}+\mathbf{q}n'}^\dagger \hat{c}_{\mathbf{k}n} \left(\hat{a}_{\mathbf{q}j}^\dagger + \hat{a}_{-\mathbf{q}j} \right), \quad (26)$$

with a slightly simplified electron-phonon coupling constant given by

$$g^{\text{cFr}}(\mathbf{q}j, \mathbf{k}n') = \frac{1}{q} \frac{4\pi}{\Omega_0} \left(\frac{1}{2\omega_{j\text{LO}} V_{\text{BvK}}} \right)^{1/2} \frac{p_{j\text{LO}}}{\epsilon^\infty} \times \sum_m s_{n'm}(\hat{\mathbf{k}}') (s_{nm}(\hat{\mathbf{k}}))^*. \quad (27)$$

The suppression of the “ i ” prefactor from Eq. 16 to Eq. (27) is related to the Born and Huang convention³⁵. Still working in the lowest order of perturbation theory, Eq. (18) can be re-written as a linear combination of α_j parameters and phonon frequencies at Γ ,

$$\text{ZPR}^{\text{cFr}} = -\sigma \sum_j \alpha_j \omega_{j\text{LO}}, \quad (28)$$

with each α_j being

$$\alpha_j = \frac{\langle (m_n^*(\hat{\mathbf{q}}))^{\frac{1}{2}} \rangle_{\hat{\mathbf{q}}n}}{\epsilon_j^* \sqrt{2\omega_{j\text{LO}}}} \quad (29)$$

] The numerator is purely electronic, and independent of the j index, while the denominator is purely dielectric and dynamical. This simplification appears only for the cubic crystallographic system. A similar decoupling appears for the polaron energy:

$$E_P = - \langle (m_n^*(\hat{\mathbf{q}}))^{\frac{1}{2}} \rangle_{\hat{\mathbf{q}}n} \left(\sum_j \frac{\sqrt{\omega_{j\text{LO}}}}{\epsilon_j^* \sqrt{2}} \right). \quad (30)$$

These equations shed light on the relationship between the standard and generalized Fröhlich model. They will provide guidance for the choice of the parameters for the standard Fröhlich model, which follows in the next section.

D. Effective masses

An automatic python workflow was created to obtain the electronic effective masses and store them in a database. The input files for ABINIT^{22,38} were generated using AbiPy^{22,38} by inserting the ground-state parameters from the Materials Project database. The valence band maximum (VBM) and conduction band minimum (CBM) were then determined by AbiPy by producing the electronic band structure along the high-symmetry paths

of each system's Brillouin zone. The effective mass tensors at these points were determined by calculating the second order derivative of the VBM and CBM eigenenergies with respect to the wavevector \mathbf{k} , including the effect of band degeneracies and warping³³, within Density Functional Perturbation Theory (DFPT)³⁹, as implemented in ABINIT.

In section III, we use the directional average of effective masses,

$$m^* \approx \left(\langle (m_n^*(\hat{\mathbf{q}}))^{\frac{1}{2}} \rangle_{\hat{\mathbf{q}}_n} \right)^2, \quad (31)$$

to facilitate the characterization of the materials. For cubic systems, this expression accounts exactly for the anisotropy in the effective masses and for the possible degeneracies, as discussed in Sec. II C. For non-cubic systems, there is no such decoupling of the effective mass factor from the dielectric and dynamical ones, as Eq.(25) is not exact.

III. HIGH THROUGHPUT RESULTS

A. Standard Fröhlich model

The standard Fröhlich model relies on the ω_{LO} frequency, the m^* effective mass and the ionic part of the dielectric tensor, ϵ^* . They combine to deliver the α parameter, and to predict a polaron formation energy E_{P} (or ZPR) obtained in the full range of values from diagrammatic Monte Carlo or Feynman path integral approaches^{25,26}. If we want to define a standard Fröhlich model for a given material, we must extract a single LO phonon frequency, an isotropic dielectric tensor and a single mass, while this situation applies exactly only to the simplest materials, namely binary (and some ternary cubic) materials with the electron or hole pockets situated at Γ . The standard Fröhlich model has nevertheless been widely used.

In order to extract such simplified parameters in a high-throughput approach, and compare to the generalized Fröhlich model and the AHC first-principles treatment, we work with the following hypotheses.

For the dielectric constants we use $\epsilon = \text{Tr}(\epsilon_{\alpha\beta})/3$. The single phonon frequency ω_{LO} is assumed to be the highest phonon frequency at Γ . For all the simple materials mentioned above, this is indeed the case (the highest frequency mode is always an LO). When several LO phonon modes are present, one could expect that the highest one has the largest LO-TO splitting and, thus, interacts most strongly with the electrons. We will see, however, that there are cases for which the highest mode is weakly coupled to electrons, and other LO modes are dominant (see the metal-azides below as an example of such a situation).

As stated in Section I, there are 1260 materials for which all necessary quantities are present to compute the ZPR^{sFr} and α using Eqs. (3) and (9). In Fig. 1 we show the dispersion map of these quantities for both valence

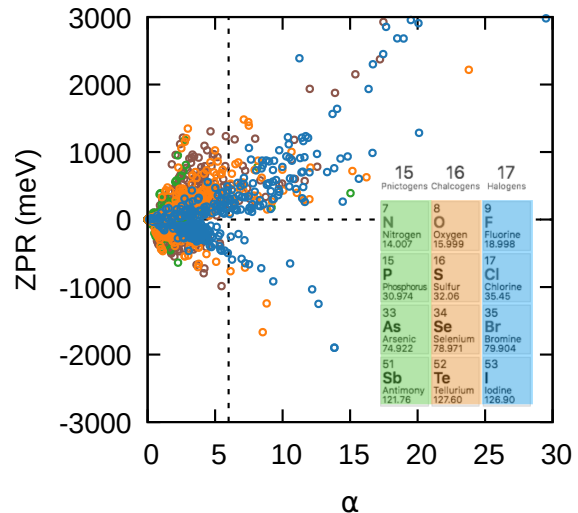


FIG. 1: Conduction (negative) and valence (positive) standard Fröhlich model ZPR and α values, for all materials except 39 (1) exceeding 3000 meV for valence (conduction) ZPR. The ZPR values are determined based on the full range coupling strength described in Eq. (7). The color corresponds to chemical elements from groups 15 to 17 of the periodic table (see inset), and brown for all other compounds. Most compounds that exhibit large values of α have at least one element from group 17. Valence values are distributed over a wider range of α , and conduction values are more concentrated below $\alpha = 10$. The vertical dashed line is at $\alpha = 6$.

and conduction band edges. The color of each point indicates the presence of an element of a given group of the periodic table (as shown in the inset), according to the following order of precedence: blue for materials with an element from group 17 (halides); if no halide is present, orange for materials with elements from group 16 (chalcogenides); green for materials with an element from group 15 (pnictogens); red for materials with an element from group 14. If no element of any of these groups is present, the circle is brown.

Values of α for conduction states are almost entirely concentrated in the $\alpha < 10$ region, while valence values extend further into the $10 < \alpha < 20$ range. This difference comes from the different distributions of bare effective masses for conduction and valence band edges⁴⁰ (shown in the top panel of Fig. 2), since ϵ^* and ω_{LO} are the same for a given material. The ZPR distributions for both valence and conduction states follow a similar distribution, with few absolute values of conduction ZPR above 1000 meV, while the [1000,3000] meV range for absolute ZPR values is more populated in the valence case.

The broad trend ZPR that is proportional to α in a family is visible for both conduction and valence bands, coming from the simple proportionality through the ω_{LO} frequency in the lowest order of perturbation theory. Not

all chemical families show the same slope, even if the group of constituting element is taken into account, because the nuclear mass and bonding vary within a group, which can strongly influence ω_{LO} and ϵ^0 .

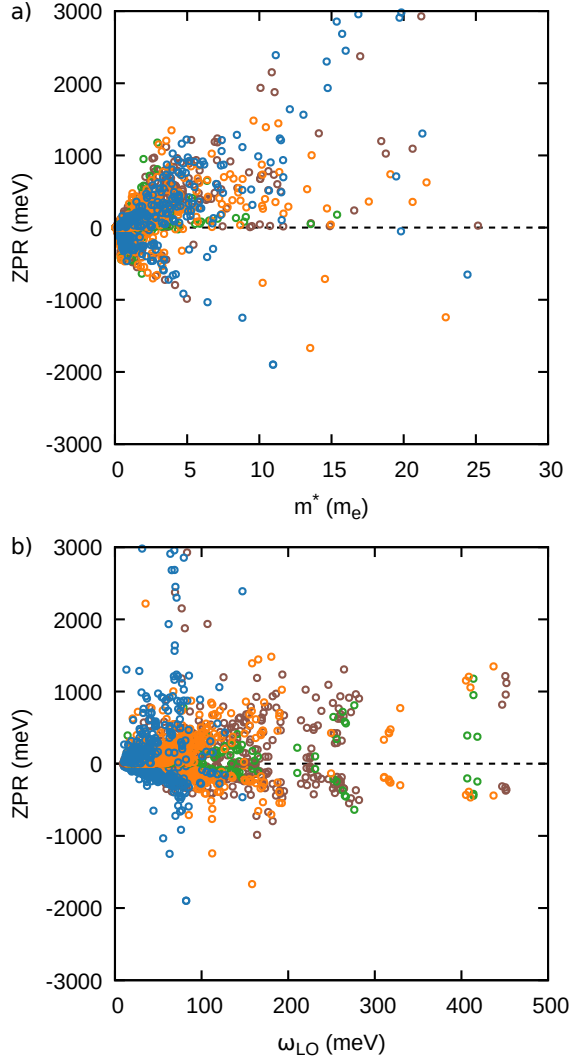


FIG. 2: Dispersion of conduction (negative) and valence (positive) standard ZPR energies versus the effective mass, m^* (top), and phonon frequency, ω_{LO} (bottom) for all materials with ZPR below 3000 meV. Same conventions as in Fig. 1. A rough square root behavior (Eq. (10)) governs the maximum accessible ZPR for a given mass, and a degree of clustering is visible of the frequencies as a function of chemical period, with the lowest frequencies for halides, followed by chalcogens, then the remaining materials. Dependence with the band effective mass (Eq. (31)) shows a dominant linear behaviour, with a wider dispersion for valence bands when compared to the conduction band masses.

Halides (group 17) produce the highest values of α , far beyond the limit of validity of the perturbation treatment. Then the chalcogenides show the next set of large

values of α , followed by the pnictogens and compounds with elements of group ≤ 14 , with the lowest α . This trend is chemically intuitive as halides have a stronger polar behavior than elements of previous groups: polaron binding grows with electron affinity, but compounds from the “other” category, with no strongly electrophilic element, can be found in the full range up to quite high $\alpha \sim 20$.

By looking at Eqs. (3), (4), and (9) we split the descriptors into two categories: electronic properties with $1/\epsilon^\infty$ and m^* ; and vibrational properties, $1/\epsilon^*$ and ω_{LO} . Of these, only m^* and ω_{LO} show clear clustering or trends, see Fig. 2. The data shown in these figures allows to further understand the dispersion of values shown in Fig. 1. On the one hand, the highest values of m^* and $1/\epsilon^\infty$ are obtained in halides, followed by chalcogens, which contributes to their large values of both α and ZPR. The largest effective masses come from transition metal halides where the conduction band is an empty d-band, isolated due to crystal field splitting, which can become extremely flat (e.g. CaTiF_6). Regarding the dependency of ZPR on ω_{LO} shown in Fig. 2 b), two points must be mentioned. The first concerns the outliers with $\omega_{LO} > 300$ meV. All these systems have one or more hydrogen atoms, leading to high frequency non-dispersive phonon modes (molecular-type vibrational levels). This alone does not necessarily result in large values of α , but in the presence of halides or chalcogens the valence band mass also tends to increase, which does lead to large values of ZPR. The second point is that materials with one or more halides are concentrated at the lower end of the distribution in phonon frequencies, but this is compensated by the other parameters which are electronic, leading to both large α and ZPR. The conduction bands of these materials do not possess such heavy masses, and so the ZPR ends up being smaller.

A general trend can be derived from the datasets: the values of α and ZPR will increase if more polar elements are present in the compound, especially halides. These produce large band effective masses and electronic dielectric constants, and so smaller ϵ^* . Despite lower values of ω_{LO} , the α in halides is often beyond the limit of validity of perturbation theory for the standard Fröhlich model, indicating the probable breakdown of the first-principles AHC approach.

In addition to the analysis of the validity of perturbation theory thanks to limits on α , the validity of the large polaron hypothesis can also be assessed. This hypothesis is crucial for the Fröhlich approach, be it in the standard form or in the generalized form. For this purpose, the polaron radius, Eq. (14), is computed, in the strong-coupling approximation. Such information is combined with the α data for both conduction and valence band edges in Fig. 3. Histogram distributions of α and a_p values are shown. An indicative value of $a_p = 10$ Bohr has been chosen to indicate the frontier between small polarons and large polarons. Similarly, and as already discussed, values of α larger than 6 loosely indicate

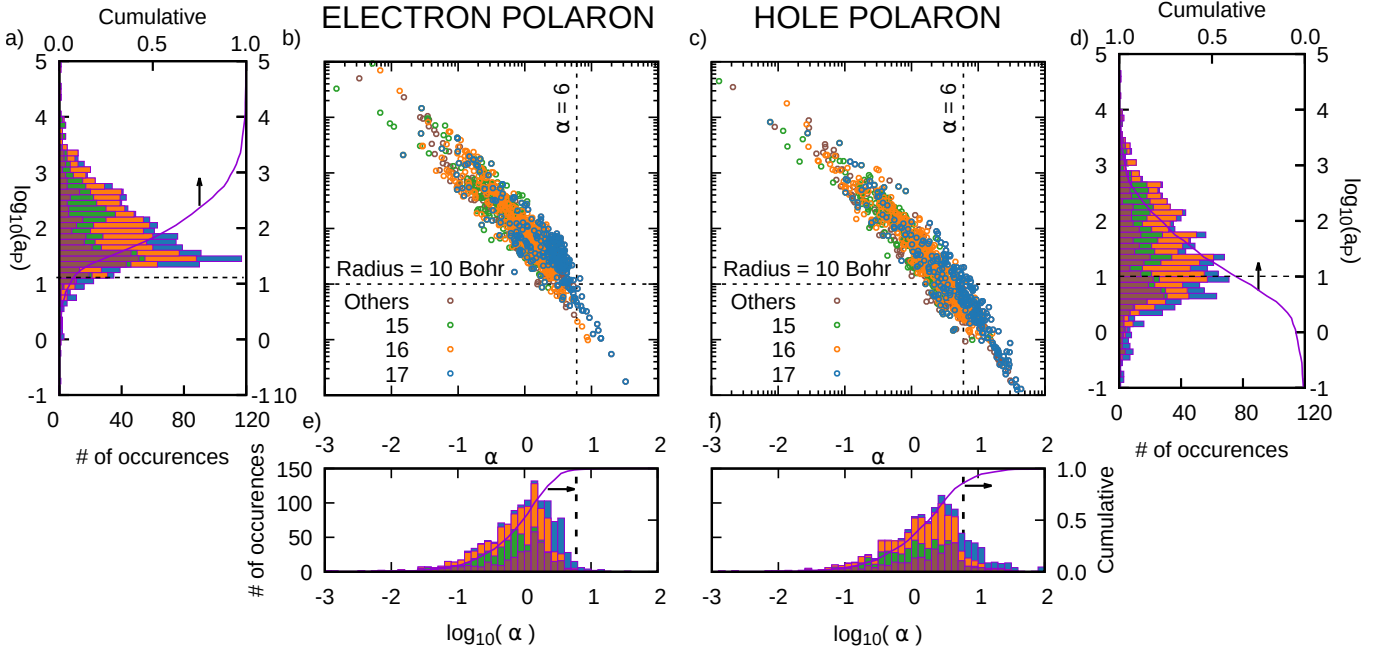


FIG. 3: Polaron radii and α distributions for both holes and electrons within the standard Fröhlich model. Dashed lines show the limits of Fröhlich perturbation theory ($\alpha = 6$) and small polarons (indicatively $a_p = 10$ Bohr). Hole polarons are clearly heavier and more localized, but the majority of both distributions is within the limits of validity of the Fröhlich model. Histograms show the statistical and cumulative distribution, with stacked bar graphs for the different chemical periods. See Table S.5 for the distribution of radii and coupling strength of both electron and hole polarons. Same color code as in Fig. 1.

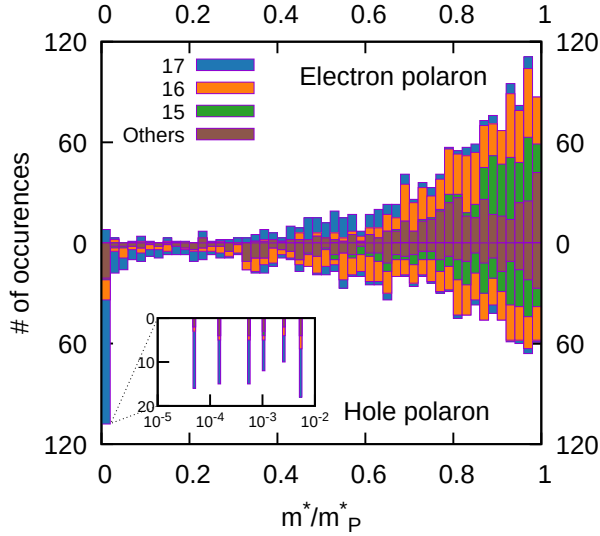


FIG. 4: Inverse effective mass enhancement, for both hole (positive) and electron (negative) polarons within the standard Fröhlich model. Stacked bars correspond to chemical period. The inset shows the distribution for very heavy hole polarons with huge mass enhancement.

The effective mass enhancement is based on the mapping provided the Diagrammatic Monte Carlo results (see Fig. 5 in Ref. 26) and Eq. (12). Same color code as in Fig. 1.

breakdown of perturbation theory. Materials with small a_p will not be well reproduced with the long-range, large polaron Fröhlich approximation. See Table S.5 for the statistics of both electron and hole polarons. The number of cases yielding large polarons that can be described by perturbation theory is quite high: about 91% of the materials for electron and 58% for hole polarons. The large polaron hypothesis breaks down for about 5% of cases, for electrons and 34.5% of the hole polarons. The remainder, namely, materials for which the large polaron hypothesis is valid, but for which perturbation theory breaks down is very small: only 0.08% for the electron polarons, and 0.56% for the hole polarons.

The EPI enhancement of the bare electronic effective mass is shown in Fig. 4. The contribution is determined based on the diagrammatic quantum Monte Carlo calculation proposed by Mishchenko et al. (see Fig. 5 in Ref. 26). Considering the improved generalized Fröhlich model, polaron anisotropy will shift many materials to lower critical radii, and the breakdown of perturbation theory can occur at lower α , as shown in Ref. 36, where a similar analysis of repartition of α and a_p was performed for a much smaller set of materials, all exhibiting cubic symmetry.

On this basis, the large polaron hypothesis with perturbative treatment might still be appropriate to treat the electron polaron for a majority of materials, but this might not be true to treat the valence band. The break-

down of perturbation theory for α bigger than 6, implying also that first-principles AHC theory would be inappropriate, is less often encountered, even for valence bands.

B. Generalized Fröhlich model

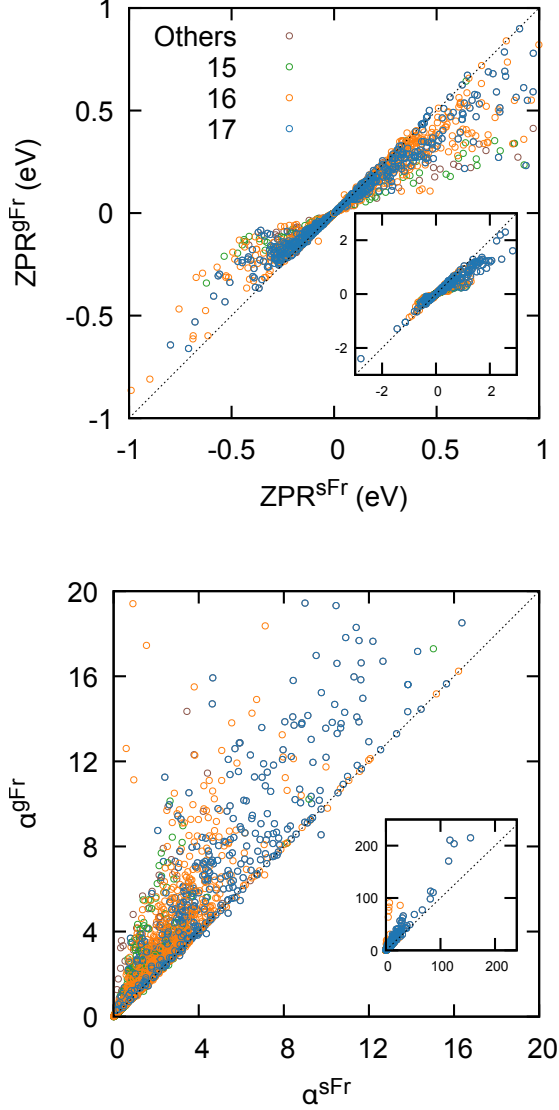


FIG. 5: Comparison of generalized and standard Fröhlich model for ZPR (top) and α (bottom), for both valence and conduction edges. The insets show the dispersion for the full range of values of ZPR and α .

The generalized ZPR is clearly smaller than the standard Fröhlich model, often by a factor of 2 or more, whereas the α_S and α_G are quite close, with slightly larger α_G values. This shows that different factors influence the ZPR and α .

We now compare our results to the generalized Fröh-

lich model discussed in Section II B. Here we define the direction-dependent dielectric tensor as $\epsilon^\infty(\hat{\mathbf{q}}) = \sum_{\alpha\beta} \hat{q}_\alpha \epsilon_{\alpha\beta}^\infty \hat{q}_\beta$, we take into account all phonon modes with their respective direction dependence $\omega_{j0}^*(\hat{\mathbf{q}})$ and coupling, $\epsilon_j^*(\hat{\mathbf{q}})$, and the direction-dependent effective mass inside Eq.(17). To evaluate the directional dependence, all quantities that depend on $\hat{\mathbf{q}}$ are computed on a sphere of radius 10^{-4} Bohr $^{-1}$, using a total of 2000 points to sample the sphere. The phonon frequencies and eigendisplacements are interpolated on this grid using the *anadbb* tool in the ABINIT software package. Note that all parameters (e.q. k-point grids, energy cutoffs, pseudo potentials) are the same for the evaluation of all quantities involved. Differences that arise will come only from the nature of each method, namely that in the generalized model the angular dependency of all quantities is taken into account and the effects of all phonon modes are included, weighted by the mode-polarity vectors.

For the generalized Fröhlich model, no all-range calculations of the Feynman or DMC type have been performed until now. We have thus to rely on the perturbative result, Eq. (24), to obtain the ZPR. Coherently, the lowest order of perturbation, Eq. (10), is used to compare with the standard Fröhlich model. For α in the generalized Fröhlich model, we employ the expression

$$\alpha_G = \sum_j \langle \alpha_j(\hat{\mathbf{q}}) \rangle_{\hat{\mathbf{q}}}, \quad (32)$$

with $\alpha_j(\hat{\mathbf{q}})$ given by Eq. (21).

In Fig. 5 we show the comparison between the standard and the generalized Fröhlich model ZPR, both obtained in low-order perturbation theory, that we denote ZPR_S and ZPR_G, respectively, and α , that we denote α_S and α_G , respectively. While it is not apparent to the naked eye, ZPR values for binary cubic systems match in both the generalized and standard models (see the file *binarycubicZPRcomparison.json* provided as SI). From Fig. 5 it is apparent that the generalized model reduces the value of the ZPR, in some cases drastically. For instance the valence ZPR goes from 3164.39 meV to 548.18 meV for Rb₂HBrO, a difference of 82%, and the conduction ZPR of Li₂CaHfF₈ goes from 3484.27 meV to 2177.84 meV, a difference of 37%. For Rb₂HBrO the reason for this drastic reduction comes from the mode polarity vectors, which re-weight the contribution of each phonon mode, and the vibrational molecular modes arising from the presence of hydrogen atoms see their contributions diminished, so the $\alpha_j(\hat{\mathbf{q}})$ factor in Eq. (18) cancels the very high mode frequency. This also occurs for other outlying compounds of Fig. 1.

For the conduction bands, the relative reductions of the largest ZPR_G values are much smaller in comparison, with a 37% reduction for Li₂CaHfF₈ and 39% for K₂TiF₆, i.e. those with the largest ZPRs. While some re-weighting happens thanks to the mode-polarity vectors, these materials have massive, almost point-defect-like, conduction bands. The main contribution to the

reduction will then come from the fact that we account for the geometry of the Brillouin zone in the integration.

Finally we look at how α_G compares to α_S in Fig. 5 b). The outlying material for both conduction and valence cases is CsNO_2 , which has both heavy conduction and valence band masses and high-frequency phonon modes. However, the largest $\alpha_j(\hat{\mathbf{q}})$ contributions that enter into Eqs. (18) and (21) are from modes at much lower frequencies. While this delivers a large α_G , it does not make this material an outlier in terms of ZPR_g , and illustrates how mode and direction independent quantities are not fully reliable and can fail in some cases. Nevertheless, for all other materials the differences between α_G and α_S are within 50% of α_S .

Some interesting outliers were found when scanning through the values of ZPR and α in both models for binary compounds, including a family of alkali metal nitrides with the chemical formula XN_3 . These are discussed in the next sections, together with other materials which have large ZPR due to a high number of fluorine ions, comparing to benchmark results from a fully first-principles method.

IV. AB INITIO BENCHMARKING

The generalized Fröhlich model is expected to improve over the standard model. In order to quantify the improvement brought by the generalized Fröhlich model, we compare model results with fully ab initio (AHC) calculations of the ZPR. As the latter are much more costly, we have selected a limited set of representative and/or simple test cases. Like the generalized Fröhlich model, the first-principles AHC approach works in the lowest order of perturbation.

A. Results and comparison to Miglio et al.

Previously, Miglio et al.⁹ computed ZPR from first principles for a set of 30 materials and compared them with the generalized Fröhlich model. Most of the stronger ionic compounds (oxides and chalcogenides) were well described by the model, within 25% error compared to the first principles AHC approach. For nitrides, the ZPR were less accurate but still within 50% error. Their ZPR was twice larger in first principles calculations than using the generalized Fröhlich model. We calculate the valence band ZPR for an intersecting subset of 20 materials (Tab. S.6) based on the generalized ZPR for cubic materials, Eq. (30).

In addition, we have chosen specific systems with high ZPR, combined with either low, medium or high α . Despite our theories being based on a perturbative approach, the latter case is nevertheless instructive as it is expected that the similarity or difference within a common perturbative framework of similar order will translate to a similarity or difference within more elaborate

frameworks able to tackle non-perturbative behaviors. The first case of lower α are four ionic molecular crystal azides: KN_3 and RbN_3 crystallize in a tetragonal system, LiN_3 and NaN_3 in a monoclinic system; the following case contains the trigonal system CsNO_2 (medium α); and, for the final extreme case we examine cubic $\text{Cs}_2\text{NaScF}_6$, tetragonal $\text{Li}_2\text{CaHfF}_8$ and trigonal K_2TiF_6 .

In Fig. 6 we see that overall the standard Fröhlich model overestimates the non-adiabatic AHC ZPR, while the generalized Fröhlich model underestimates it. The former relies solely on the contribution from the highest ω_{LO} phonon branch. The latter accumulates the contribution to the ZPR from all the LO-phonon modes, and the properties are averaged for all directions $\mathbf{q} \rightarrow 0$.

There are still important contributions missing from the generalized Fröhlich model, such as the non-polar and TO phonon modes, but the trend is surprisingly strong in both cases: the dominant qualitative physics is already present in the standard Fröhlich model, and, in most of the cases, the generalized version quantitatively corrects the ZPR.

The systems $\text{Cs}_2\text{NaScF}_6$ and $\text{Li}_2\text{CaHfF}_8$ are the only cases in which the calculated values do not all follow this global trend. Their values in the standard and generalized models are very close due to a low ω_{LO} . Even if the ZPR is spread over other phonon modes, their frequency would not be far from the low ω_{LO} . In SI Table S. 2, we average ω over the phonon modes using the ZPR as weight. The farther this average is from ω_{LO} , the higher is the importance of phonons at lower frequencies

The main parameters of the standard and generalized Fröhlich approaches are shown in SI Table S. 1 and in Table S. 2, respectively, for our benchmark materials.

In the following Secs. IV B and IV C for KN_3 and $\text{Cs}_2\text{NaScF}_6$, we determine the features which produce differences between the standard and generalized Fröhlich approaches, and with the non-adiabatic AHC method.

B. Azides: large ZPR, small α

For the azide series, the highest ω_{LO} are similar with a maximum difference of 14 meV. Therefore, the changes in the ZPR come from the dielectric constant and the effective mass. The trend from Rb, K, Na to Li is a decrease of ionic radius and an increase of electronegativity⁴¹, leading to a decrease of the unit cell volume and the dielectric constant, and an increase of the effective mass.

In the standard Fröhlich model the value of α of KN_3 is smaller than, for example, the KF system. Even if both have a similar fraction $\sqrt{m^*}/\epsilon^*$ (0.25 for KF and 0.28 for KN_3) KN_3 has a higher ω_{LO} (271 meV), see SI Table S.3 or SI Fig. S.4 than KF (42 meV). The very high ω_{LO} of KN_3 comes from the resonances created by the linear chains of N_3 harmonic oscillators, where all three atoms vibrate along the bonds. The same reasoning can be applied to the other azides.

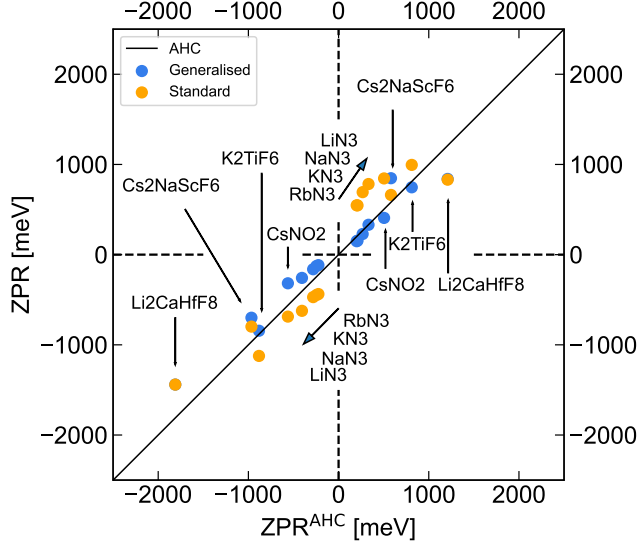


FIG. 6: Comparison of the VBM (positive, right top part) and CBM (negative, left bottom part) ZPRs between the standard and generalized Fröhlich models and the non-adiabatic AHC approach for some chosen systems.

In our choice of parameters for the standard Fröhlich model, the system LO phonon mode with the highest frequency is selected as the sole contributor to ZPR, which is not the case for the generalized Fröhlich model. In the case of KN_3 , there are two active LO phonon modes in the generalized Fröhlich approach (see bottom of SI Table S.3). The phonon mode with highest contribution (76%) to the ZPR is LO phonon mode $j=15$ with a frequency of 20 meV, and not the highest LO mode ($j=24$) with a frequency of 260 meV. As the contribution for the ZPR changes from the highest LO mode to a lower one, the value of α also changes as it is explicitly proportional to the phonon frequency by $\omega_{\text{LO}}^{-1/2}$ both for standard and generalized Fröhlich, Eqs. (3) and (21) respectively. The renormalization including all LO modes translates a low $\alpha = 2.03$ for the standard Fröhlich model into a higher $\langle \alpha_j(\hat{\mathbf{q}}) \rangle_{j\hat{\mathbf{q}}} = 5.09$ using the generalized Fröhlich model. The value of α can nonetheless also be lower in a few cases for the generalized Fröhlich model (see Fig. 5), as the re-distribution of the ZPR to other phonon modes can be compensated by effective mass anisotropy or band degeneracy effects.

Going beyond the generalized Fröhlich approach and deconstructing the non-adiabatic AHC ZPR into its phonon mode components (see top of SI Table S.3), we find that the highest contribution of 26.14% to the total ZPR comes from LO phonon mode 15 and that there are non-LO phonon modes (20, 21 and 22, excluded from the Fröhlich models) which have even higher contribution to

the ZPR than the highest frequency LO phonon mode 24.

Several factors contribute to the spread of the ZPR contribution throughout the different phonon states. One key attribute is the polarizability and eigenvectors of the modes. Phonon mode 15 in KN_3 has a stronger polarizability than the highest phonon mode, which is mostly driven by the lightest atoms. Mode 15 has a mix of contributions between the potassium and nitrogen atomic vibrations, with larger dipoles, and hence a larger mode polarizability.

A second key factor is the inclusion of non-LO modes. In Fig. 7, we show the electron self-energy of KN_3 (bottom) and the spectral function (top). The LO-phonons can be found in the self-energy with characteristic Fröhlich peaks⁴². Specifically in KN_3 , the self-energy terms for phonon modes 15 and 24 show a peak at their Γ point phonon frequency (the KS energy is at 0.0 eV). Mode 17 is also LO, but the peak amplitude is small, around 1 meV. In addition to their contribution to the ZPR binding energy, the LO-phonon modes are also responsible for satellites in the spectral function visible in the top panel.

The non-LO phonon modes (either TO or non-polar) do not show peaks but a type of plateau starting at their Γ point phonon frequencies, linked to long-range quadrupole potential^{43,44} and/or short-range fields⁴⁵. At the KS energy, where the ZPR is evaluated, their $\text{Re}\Sigma(\varepsilon)$ is not negligible at all, with a net contribution larger than that of the LO modes.

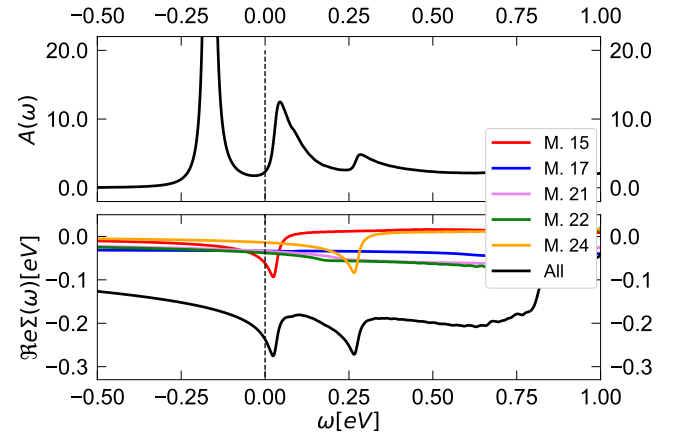


FIG. 7: Spectral function, $A(\omega)$ (top) and the real part of the self-energy, $\text{Re}\Sigma(\omega)$ (bottom) for KN_3 at the CBM. The self-energy is split by phonon mode for the largest contributions to the ZPR_c as in SI Table S.3.

Another way to distinguish contributions to the ZPR is by plotting their dependency on the phonon wave-vector (norm), as in Fig. 8. The two LO phonon modes have their main contributions from wave-vectors close to Γ , and correspond to long-range electric dipole fields. The non-LO phonon modes ($j=17, 21$, and 22) originate at the boundary of the Brillouin zone, and correspond to inter-

actions with shorter-range crystal fields. We note that it is important in this analysis to avoid mixing LO and non-LO band contributions when their frequencies cross away from Γ , by following the irreducible representations and character of each mode to attribute the $\text{ZPR}(j, \mathbf{q})$ contributions.

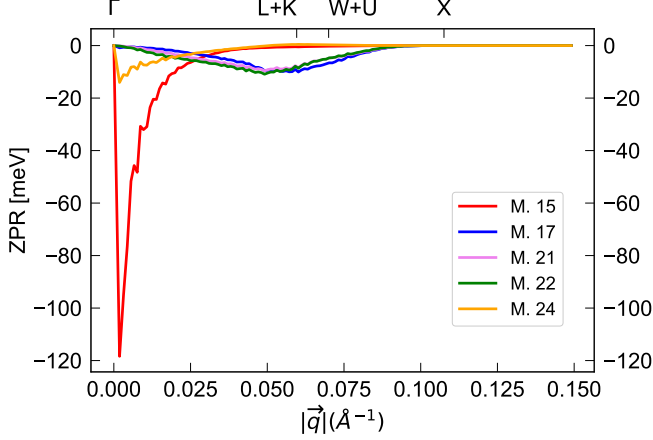


FIG. 8: Spherical accumulation of the ZPR_c of KN_3 as a function of the norm of the vector $|\mathbf{q}|$ for each phonon mode using the $64 \times 64 \times 64$ \mathbf{q} -grid sampling. The norms of selected high symmetry points are shown on the top axis.

C. $\text{Cs}_2\text{NaScF}_6$: large ZPR, large α

The ZPR_c of the $\text{Cs}_2\text{NaScF}_6$ compound is much higher than the azides with a value of -966.1 meV in the non-adiabatic AHC. In addition to the small increase of the effective dielectric constant contribution, there is also an approximately 8-fold increase of the effective mass compared with the azides (SI Table S. 1). The $\text{Cs}_2\text{NaScF}_6$ electron band structure and the projected density of states are shown in SI Fig. S.5. The bottom conduction band has very low dispersion which translates into a large effective mass and localized electrons, which are found in the Sc-F bonds. The main source of the high ZPR is the coupling between the (high frequency) vibrations of F atoms and the d-orbital conduction band of Sc.

Dissimilar to the azides, both the standard and the generalized Fröhlich models underestimate the non-adiabatic AHC ZPR_c of the $\text{Cs}_2\text{NaScF}_6$ compound by 168 and 267 meV, respectively. Surprisingly, the generalized Fröhlich model gives worse result than the standard when comparing to the non-adiabatic AHC approach, through a compensation of errors between neglecting lower frequency LO modes and neglecting non-LO modes altogether. The ZPR calculated within the generalized Fröhlich and non-adiabatic AHC can be split into phonon mode contributions (SI Table S.4). Unlike

the case of the azides, the highest ZPR contribution is the non-LO phonon mode 29, contributing almost 45% and an α_i of 9.20. Generalized Fröhlich ignores the non-LO phonons, which, in this case, are close to the ω_{LO} . Part of this contribution is spread to lower LO phonon modes leading to a worse ZPR.

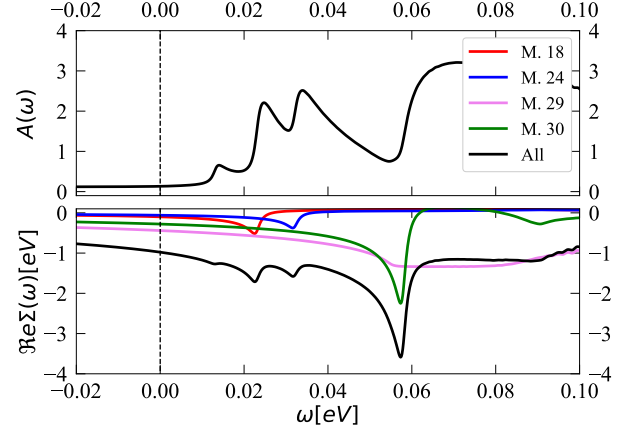


FIG. 9: Spectral function, $A(\omega)$ (top) and the real part of the self-energy, $\Re\Sigma(\omega)$ (bottom) for $\text{Cs}_2\text{NaScF}_6$ at the CBM. The self-energy is split by phonon mode for the largest contributions to the ZPR_c as in SI Table S.4. The frequency range is limited to the satellites: the two QP peaks at -0.249 and 0.341 eV are not visible in this range. The first peak in $A(\omega)$ comes from a mode with low contribution to the full ZPR, which is only a small bump in the total $\Re\Sigma(\omega)$.

The real part of the self-energy for phonon mode 29 is the most important at the KS energy (0.0 in Fig. 9), and increases towards its Γ -point phonon frequency (47.8 meV) but it has no peak. The phonon mode with the highest frequency is a LO phonon mode, showing a green peak in the self-energy figure, but has a smaller contribution of around 28.5% to the total ZPR. The other phonon modes shown in the figure are also LO phonon modes and have small self-energy peaks at their Γ point phonon frequencies. The spectral function shape is complicated by the presence of two quasi particle solutions (not visible in the figure), which convolute the full self-energy. This is more common in the electron-phonon case (as opposed to electron-electron) as the self-energy amplitude is of the same order of magnitude as the phonon energies (or even larger).

The angle-integrated ZPR as a function of wave-vector norm (Fig. 10) shows the Fröhlich-like behavior close to $|\mathbf{q}| = 0$ for $j = 18, 24$, and 30. Mode 29 behaves as $|\mathbf{q}|^2$ following the volume contribution $4\pi|\mathbf{q}|^2$ in the angular average, which means the ZPR contributions are relatively constant throughout the Brillouin zone.

As a summary for the set of “extreme” materials considered this section, we observe that the standard and generalized Fröhlich models are both close to the full

first principles trend, but overestimate and underestimate, respectively, the non-adiabatic AHC ZPR. One characteristic of high ω_{LO} materials, as in the azides, is the geometrical isolation of the lighter atoms. If lower frequency phonon modes have high polarization, the generalized Fröhlich ZPR is spread over these modes, reducing the ZPR compared with the standard Fröhlich model, which includes solely the highest ω_{LO} phonon mode. This spread also leads to an increase of the averaged α value, as the electrons interact with lower frequency phonon modes. In cases with intrinsically low ω_{LO} phonon modes, the ZPR can be similar for both models. In addition, ignoring non-LO modes can worsen the generalized Fröhlich model results, especially if the non-LO phonon mode is close to ω_{LO} , exaggerating the importance of lower frequencies and widening the distance from the non-adiabatic AHC ZPR.

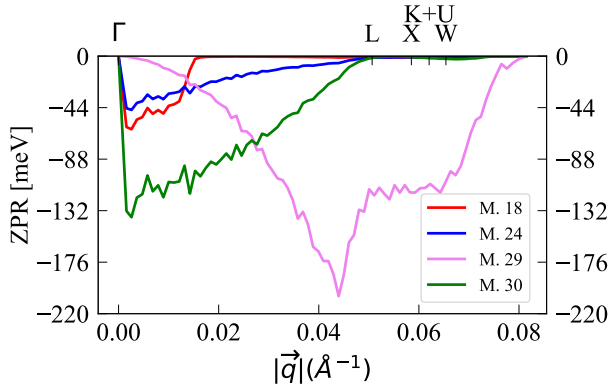


FIG. 10: Spherical accumulation of the ZPR_c of $\text{Cs}_2\text{NaScF}_6$ as a function of the norm of the vector $|\vec{q}|$ for each phonon mode using the $64 \times 64 \times 64$ \vec{q} -grid sampling.

V. CONCLUSIONS

We evaluate the polaron binding energy, or zero point renormalization, in both standard and generalized Fröhlich models for a database of 1260 materials. Lowest order perturbation theory is used for the generalized Fröhlich model, while both perturbative and all-range formulas are available for the standard model, once the single parameter α is defined.

In our study we find a broad range of validity for both models (58% of valence bands and 91% of conduction band polarons), but the generalized model is in better quantitative agreement with our fully ab initio spot checks using the Allen-Heine-Cardona theory. The gen-

eralized Fröhlich model ZPR shows a significant decrease of the ZPR but a slight increase of α with respect to the standard model. We find distinctive trends depending on the material's composition: more electronegative compounds containing halides or chalcogens generally present higher ZPR associated with higher α , while compounds containing group 13 elements show rather lower ZPR, though there are outliers in all categories.

Given the broad range of behaviors in our set of materials, we complement our studies with fully ab initio DFT-based non-adiabatic AHC calculations of the ZPR. We focus on few outlier materials with different α (low, medium, and high) and high ZPR. Both Fröhlich models follow the trend of the non-adiabatic AHC qualitatively. The lower and medium α materials show a quantitative improvement going from standard to generalized Fröhlich, thanks in particular to the redistribution of the ZPR to lower frequency phonon modes. In some exceptional cases (e.g. $\text{Cs}_2\text{NaScF}_6$) the standard Fröhlich can give better (i.e. closer to AHC) results than the generalized model, when important non-LO phonon modes are ignored.

The standard Fröhlich model can fail in more than one way: due to essential non-LO phonons modes, anisotropy, or, crucially, the breakdown of perturbation theory. However, regardless of the Fröhlich method's limitations, we provide strong evidence for the ubiquity of polaron formation, the range of possible behaviors and parameter space, and the importance of polarons in providing reliable band gaps and effective masses. In a very small number of weak coupling cases the estimated polaron radius is small enough to call into question the applicability of Fröhlich type models.

ACKNOWLEDGMENTS

This work has been supported by the Fonds de la Recherche Scientifique (FRS-FNRS Belgium) through the PdR Grant No. T.0103.19 - ALPS. ZZ and PMCM acknowledge financial support by the Netherlands Sector Plan program 2019-2023. This project has received funding from the European Union's Horizon 2020 research and innovation program under grant agreement No. 951786 - NOMAD CoE. Computational resources have been provided by the CISM/UCLouvain and the CECI funded by the FRS-FNRS Belgium under Grant No. 2.5020.11, as well as the Tier-1 supercomputer of the Fédération Wallonie-Bruxelles, funded by the Walloon Region under grant agreement No. 1117545. We acknowledge a PRACE award granting access to MareNostrum4 at Barcelona Supercomputing Center (BSC), Spain (OptoSpin project id. 2020225411). Moreover, we also acknowledge a PRACE Tier-1 award in the DECI-16 call for project REM-EPI on Archer and Archer2 EPCC in Edinburgh.

- ¹ M. Cardona and M.L.W. Thewalt. Isotope effects on the optical spectra of semiconductors. *Rev. Mod. Phys.*, 77:1173–1224, 2005.
- ² M. Shishkin, M. Marsman, and G. Kresse. Accurate quasi-particle spectra from self-consistent GW calculations with vertex corrections. *Phys. Rev. Lett.*, 99:246403, 2007.
- ³ A. Marini. Ab-initio finite temperature excitons. *Phys. Rev. Lett.*, 101:106405, 2008.
- ⁴ F. Giustino, S.G. Louie, and M.L. Cohen. Electron-phonon renormalization of the direct band gap of diamond. *Phys. Rev. Lett.*, 105:265501, 2010.
- ⁵ S. Moser, L. Moreschini, J. Jacimovic, O. S. Barisic, H. Berger, A. Magrez, Y. J. Chang, K. S. Kim, A. Bostwick, E. Rotenberg, L. Forro, and M. Grioni. Tunable polaronic conduction in anatase TiO₂. *Phys. Rev. Lett.*, 110:196403, 2013.
- ⁶ G. Antonius, S. Poncé, P. Boulanger, M. Côté, and X. Gonze. Many-body effects on the zero-point renormalization of the band structure. *Phys. Rev. Lett.*, 112:215501, 2014.
- ⁷ S. Poncé, Y. Gillet, J. Laflamme Janssen, A. Marini, M. Verstraete, and X. Gonze. Temperature dependence of the electronic structure of semiconductors and insulators. *J. Chem. Phys.*, 143(10):102813, 2015.
- ⁸ Carla Verdi, Fabio Caruso, and Feliciano Giustino. Origin of the crossover from polarons to fermi liquids in transition metal oxides. *Nature Communications*, 8:15769, 2017.
- ⁹ Anna Miglio, Véronique Brousseau-Couture, Emile Godbout, Gabriel Antonius, Yang-Hao Chan, Steven G. Louie, Michel Côté, Matteo Giantomassi, and Xavier Gonze. Predominance of non-adiabatic effects in zero-point renormalization of the electronic band gap. *npj Computational Materials*, 6(1):167, 2020.
- ¹⁰ P. Hohenberg and W. Kohn. Inhomogeneous electron gas. *Physical Review*, 136(3B):B864–B871, nov 1964.
- ¹¹ W. Kohn and L. J. Sham. Self-consistent equations including exchange and correlation effects. *Physical Review*, 140(4A):A1133–A1138, nov 1965.
- ¹² Richard M. Martin. *Electronic structure. Theory and practical methods*. Cambridge University Press, Cambridge, United Kingdom, 2004.
- ¹³ L. Hedin. New method for calculating the one-particle green’s function with application to the electron-gas problem. *Phys. Rev. B*, 139:A 796, 1965.
- ¹⁴ Richard M. Martin, Lucia Reining, and David M. Ceperley. *Interacting Electrons. Theory and Computational Approaches*. Cambridge University Press, Cambridge, United Kingdom, 2016.
- ¹⁵ Herbert Fröhlich. Interaction of electrons with lattice vibrations. *Proceedings of the Royal Society of London. Series A. Mathematical and Physical Sciences*, 215(1122):291–298, 1952.
- ¹⁶ P. B. Allen and V. Heine. Theory of the temperature dependence of electronic band structures. *J. Phys. C*, 9:2305–2312, 1976.
- ¹⁷ P. B. Allen and M. Cardona. Theory of the temperature dependence of the direct gap of germanium. *Phys. Rev. B*, 23:1495–1505, 1981.
- ¹⁸ P.B. Allen and M. Cardona. Temperature dependence of the direct gap of Si and Ge. *Phys. Rev. B*, 27:4760, 1983.
- ¹⁹ C. Verdi and F. Giustino. Fröhlich electron-phonon vertex from first principles. *Phys. Rev. Lett.*, 115:176401, 2015.
- ²⁰ F. Giustino. Electron-phonon interactions from first principles. *Rev. Mod. Phys.*, 89:015003, 2017.
- ²¹ Weng Hong Sio, Carla Verdi, Samuel Poncé, and Feliciano Giustino. Polarons from first principles, without supercells. *Phys. Rev. Lett.*, 122:246403, 2019.
- ²² Xavier Gonze, Bernard Amadon, Gabriel Antonius, Frédéric Arnardi, Lucas Baguet, Jean-Michel Beuken, Jordan Bieder, François Bottin, Johann Bouchet, Eric Bousquet, Nils Brouwer, Fabien Bruneval, Guillaume Brunin, Théo Cavignac, Jean-Baptiste Charraud, Wei Chen, Michel Côté, Stefaan Cottenier, Jules Denier, Grégory Geneste, Philippe Ghosez, Matteo Giantomassi, Yannick Gillet, Olivier Gingras, Donald R. Hamann, Geoffroy Hautier, Xu He, Nicole Helbig, Natalie Holzwarth, Yongchao Jia, François Jollet, William Lafargue-Dit-Hauret, Kurt Lejaeghere, Miguel A. L. Marques, Alexandre Martin, Cyril Martins, Henrique P. C. Miranda, Francesco Naccarato, Kristin Persson, Guido Petretto, Valentin Planes, Yann Pouillon, Sergei Prokhorenko, Fabio Ricci, Gian-Marco Rignanese, Aldo H. Romero, Michael Marcus Schmitt, Marc Torrent, Michiel J. van Setten, Benoît Van Troeye, Matthieu J. Verstraete, Gilles Zerah, and Josef W. Zwanziger. The abinit project: Impact, environment and recent developments. *Comput. Phys. Commun.*, 248:107042, 2020.
- ²³ Florian Brown-Altvater, Gabriel Antonius, Tonatiuh Rangel, Matteo Giantomassi, Claudia Draxl, Xavier Gonze, Steven G. Louie, and Jeffrey B. Neaton. Band gap renormalization, carrier mobilities, and the electron-phonon self-energy in crystalline naphthalene. *Phys. Rev. B*, 101:165102, 2020.
- ²⁴ J T Devreese. Fröhlich polarons from 0D to 3D: concepts and recent developments. *Journal of Physics: Condensed Matter*, 19(25):255201, 2007.
- ²⁵ R. P. Feynman. Slow electrons in a polar crystal. *Phys. Rev.*, 97:660–665, 1955.
- ²⁶ A.S. Mishchenko, N.V. Prokof’ev, A. Sakamoto, and B.V. Svistunov. Diagrammatic quantum Monte Carlo study of the Fröhlich polaron. *Phys. Rev. B*, 62:6317–6336, 2000.
- ²⁷ Vasilii Vasilchenko, Andriy Zhugayevych, and Xavier Gonze. Variational polaron equations applied to the anisotropic frohlich model. *Phys. Rev. B*, 105:214301, 2022.
- ²⁸ Cesare Franchini, Michele Reticcioli, Martin Setvin, and Ulrike Diebold. Polarons in materials. *Nature Reviews Materials*, 6:560, 2021.
- ²⁹ T Holstein. Studies of polaron motion: Part I. the molecular-crystal model. *Annals of Physics*, 8(3):325–342, 1959.
- ³⁰ T. Holstein. Studies of polaron motion: Part II. the “small” polaron. *Annals of Physics*, 8(3):343–389, 1959.
- ³¹ Guido Petretto, Shyam Dwaraknath, Henrique P.C. Miranda, Donald Winston, Matteo Giantomassi, Michiel J. van Setten, Xavier Gonze, Kristin A. Persson, Geoffroy Hautier, and Gian-Marco Rignanese. High-throughput density-functional perturbation theory phonons for inorganic materials. *Scientific Data*, 5:180065, 2018.
- ³² H. Fröhlich. Electrons in lattice fields. *Advances in Physics*, 3:325–361, 1954.
- ³³ A. N. Mecholsky, L. Resca, I. L. Pegg, and M. Fornari. Theory of band warping and its effects on thermoelectronic

- transport properties. *Physical Review B*, 89:155131, 2014.
- ³⁴ Gerald D. Mahan. *Many-Particle Physics*. Physics of solids and liquids. Kluwer Academic, 3rd edition, 2000.
 - ³⁵ Bogdan Guster, Pedro Melo, Bradley A. A. Martin, Véronique Brousseau-Couture, Joao C. de Abreu, Anna Miglio, Matteo Giantomassi, Michel Côté, Jarvist M. Frost, Matthieu J. Verstraete, and Xavier Gonze. Erratum : Fröhlich polaron effective mass and localization length in cubic materials: Degenerate and anisotropic electronic bands. *Phys. Rev. B*, 105:119902, 2022.
 - ³⁶ Bogdan Guster, Pedro Melo, Bradley A. A. Martin, Véronique Brousseau-Couture, Joao C. de Abreu, Anna Miglio, Matteo Giantomassi, Michel Côté, Jarvist M. Frost, Matthieu J. Verstraete, and Xavier Gonze. Fröhlich polaron effective mass and localization length in cubic materials: Degenerate and anisotropic electronic bands. *Phys. Rev. B*, 104:235123, 2021.
 - ³⁷ Carla Verdi. *First-principles Fröhlich electron-phonon coupling and polarons in oxides and polar semiconductors*. PhD thesis, U. of Oxford, Oxford, UK, 2017.
 - ³⁸ Aldo H. Romero, Douglas C. Allan, Bernard Amadon, Gabriel Antonius, Thomas Applencourt, Lucas Baguet, Jordan Bieder, François Bottin, Johann Bouchet, Eric Bousquet, Fabien Bruneval, Guillaume Brunin, Damien Caliste, Michel Côté, Jules Denier, Cyrus Dreyer, Philippe Ghosez, Matteo Giantomassi, Yannick Gillet, Olivier Gingras, Donald R. Hamann, Geoffroy Hautier, François Jollet, Gérald Jomard, Alexandre Martin, Henrique P. C. Miranda, Francesco Naccarato, Guido Petretto, Nicholas A. Pike, Valentin Planes, Sergei Prokhorenko, Tonatiuh Rangel, Fabio Ricci, Gian-Marco Rignanese, Miquel Royo, Massimiliano Stengel, Marc Torrent, Michiel J. van Setten, Benoit Van Troeye, Matthieu J. Verstraete, Julia Wiktor, Josef W. Zwanziger, and Xavier Gonze. ABINIT: Overview, and focus on selected capabilities. *The Journal of Chemical Physics*, 152:124102, 2020.
 - ³⁹ J. L. Janssen, Y. Gillet, S Ponce, A. Martin, M Torrent, and X. Gonze. Precise effective masses from density functional perturbation theory. *Physical Review B*, 93:205147, 2016.
 - ⁴⁰ Geoffroy Hautier, Anna Miglio, David Waroquiers, Gian-Marco Rignanese, and Xavier Gonze. How does chemistry influence electron effective mass in oxides? a high-throughput computational analysis. *Chemistry of Materials*, 26:5447, 2014.
 - ⁴¹ W. Gordy. New Method of Determining Electronegativity from Other Atomic Properties. *Physical Review*, 69:604, 1946.
 - ⁴² Jean Paul Nery, Philip B. Allen, Gabriel Antonius, Lucia Reining, Anna Miglio, and Xavier Gonze. Quasiparticles and phonon satellites in spectral functions of semiconductors and insulators: Cumulants applied to the full first-principles theory and the fröhlich polaron. *Phys. Rev. B*, 97:115145, 2018.
 - ⁴³ Guillaume Brunin, Henrique Pereira Coutada Miranda, Matteo Giantomassi, Miquel Royo, Massimiliano Stengel, Matthieu J. Verstraete, Xavier Gonze, Gian-Marco Rignanese, and Geoffroy Hautier. Phonon-limited electron mobility in si, gaas and gap with exact treatment of dynamical quadrupoles. *Phys. Rev. B*, 102:094308, 2020.
 - ⁴⁴ Guillaume Brunin, Henrique Pereira Coutada Miranda, Matteo Giantomassi, Miquel Royo, Massimiliano Stengel, Matthieu J. Verstraete, Xavier Gonze, Gian-Marco Rignanese, and Geoffroy Hautier. Electron-phonon beyond fröhlich: dynamical quadrupoles in polar and covalent solids. *Phys. Rev. Lett.*, 125:136601, 2020.
 - ⁴⁵ J. C. Abreu, J. P. Nery, M. Giantomassi, X. Gonze, and M. J. Verstraete. Spectroscopic signatures of nonpolarons : the case of diamond. *Phys Chem Chem Phys*, 24:12580–12591, 2022.